Article

Not peer-reviewed version

Evaluating the Impact of Engineering Works in Tidal Flats Using Time-Series Satellite Images – Case of the Mont-Saint-Michel Bay, France

Jean-Paul Deroin *

Posted Date: 29 May 2023

doi: 10.20944/preprints202305.1982.v1

Keywords: sedimentation; erosion; Sentinel 2; EOS-Aster

Article

Evaluating the Impact of Engineering Works in Tidal Flats Using Time-Series Satellite Images – Case of the Mont-Saint-Michel Bay, France

Jean-Paul Deroin [1*]

[1] Université de Reims Champagne Ardenne, Faculty of Science, UR 3795 GEGENAA; jean-paul.deroin@univ-reims.fr

* Correspondence: jean-paul.deroin@univ-reims.fr

Abstract: The Mont-Saint-Michel is known worldwide for its unique combination of the natural site and the Medieval abbey at the top of the rocky islet. But the Mont is also located within an estuarine complex, which is considerably silting up. For two decades, large-scale works were planned to prevent the Mont from being surrounded by the expanding salt meadows. The construction of a new dam over the Couesnon River, the digging of two new channels, and the destruction of the causeway were the main operations carried out between 2007 and 2015. The remote sensing approach is fully suitable for evaluating the real impact of the engineering project in both time and space, particularly the expected large-scale hydrosedimentary effects, for reestablishing the maritime landscape around the Mont. Sentinel-2 satellite data have been used for the period from 2015 to 2023. Aster data were used for the previous period covering 2000 to 2017. Aerial photographs and an ALOS scene have been also used. The remote sensing approach is based on time-series images. It allows identifying local or regional consequences and temporary or permanent effects. The migration of the different channels (especially for the new west and east Couesnon river courses) and the erosion-progradation balance of the vegetation through space and time are the main features to study. Between 2007 and 2023, the erosion of the salt meadows is significant to the south-west of the Mont (− 150 ha) but more limited to the south-east (− 65 ha). The erosion effect is limited to the immediate environment because the vegetation fringe of the uppermost tidal flat along the main dike is slightly increasing (+ 35 ha) to the west and to the east (+ 40 ha). During the same period, the sedimentation considerably increased to the north-east of the Bay, between the Bec d'Andaine, the Grouin du Sud and Tombelaine islet, which seems now facing the same silting-up problem. At this stage, the remote-sensing survey indicates mixed results for the engineering project.

Keywords: sedimentation; erosion; Sentinel 2; EOS-Aster

1. Introduction

Tidal flats are a widespread morphology and ecosystem along all coasts characterized by low-sloping and suffering the tide influence [1,2]. These areas are alternately covered and uncovered by the sea water. Fieldwork is difficult if not impossible because of difficulties such as walking slowly, crossing channels, the risk of getting stuck during the flood, sinking in mud, etc. In temperate climate zones, tidal flats include a vegetation fringe in the uppermost part known as the 'schorre', and mineral surfaces corresponding to the main part known as the 'slikke'. Due to the tidal currents, the fine particles are trapped in the 'schorre', whereas the 'slikke' presents a gradient from fine to medium sand (Figure 1).

The sea level rise and the anthropic pressure make tidal flats a very sensitive environment where any facility induces local and regional consequences. In China, the extension of the port facilities disrupts sedimentation along the Yellow Sea coast [3]. A beach nourishment project in Louisiana (USA) had impacts on the dynamics of the shoreline made of mangroves and marshes [4]. In the Po River estuary, which is not a tide-dominated delta, the importance of episodic events such as heavy floods has been highlighted [5].

Preprints (www.preprints.org) | NOT PEER-REVIEWED | Posted: 29 May 2023 doi:10.20944/preprints202305.1982.v1

Optical and radar remote sensing is particularly suitable for studying tidal flats [6–8]. Some areas have been deeply investigated such as the Wadden Sea [9–11], British flats such as the Wash, the Bristol Channel or Morecambe Bay [12], the Korean coast [13], the coast of Jiangsu Province, China [14] or the Red River estuary in Vietnam [15]. In France, the Arcachon Basin [16], the Baie des Veys [17] and the Mont-Saint-Michel Bay [18,19] have been extensively studied. The present paper deals with the Mont-Saint-Michel Bay, which has been monitored for two decades due to engineering work to restore the maritime character of the Mont. Remote sensing is the main tool, combined with some field observations.

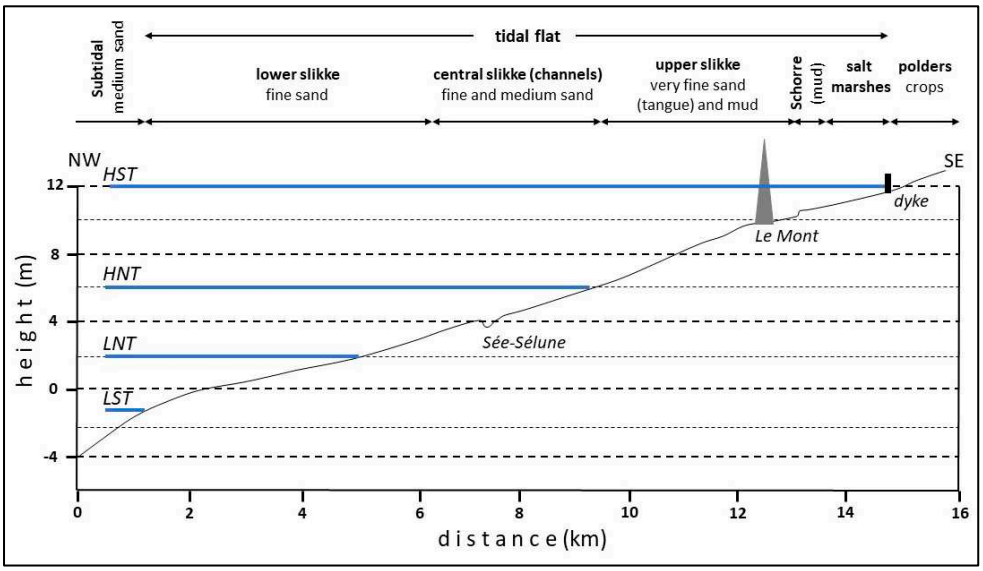

Figure 1. A NW-SE profile through the Mont-Saint-Michel Bay showing the main morphological units, their elevation, and the main sediments. The height is expressed according to the maritime scale (i.e. 0 m corresponds to about − 4 m French terrestrial maps). HNT. Highest neap tides, HST. Highest spring tides, LNT. Lowest neap tide, LST. Lowest spring tides. See also location of the profile in Figure 2.

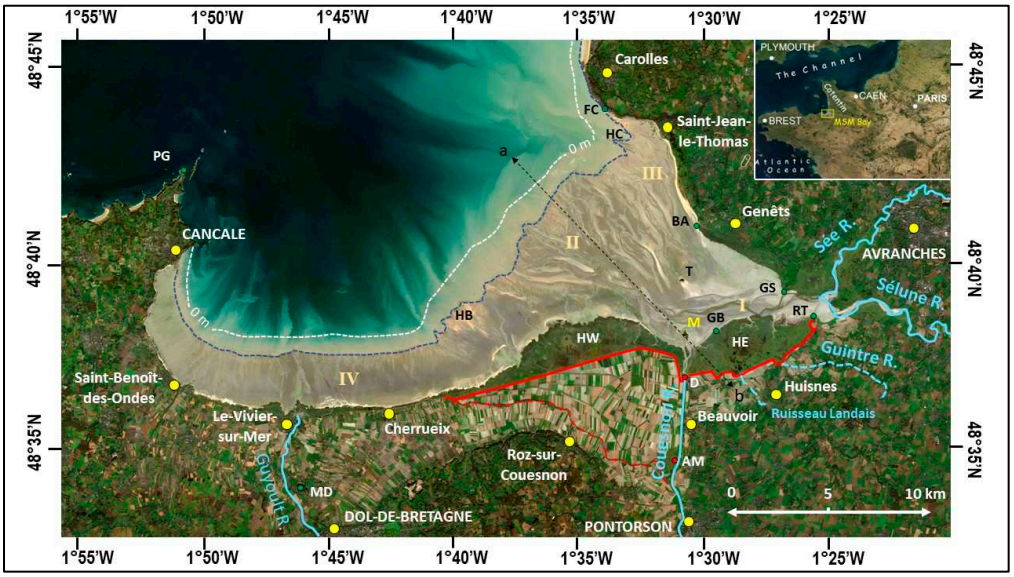

Figure 2. The Mont-Saint-Michel Bay (MSM Bay) and its tidal flats viewed with Sentinel-2 (true colour composite from the image acquired on 12 November 2020). White dashed line: Elevation is 0 m. Blue dashed line: Elevation of the sea at the time of acquisition is 3.75 m, one hour after the low tide. AM. Anse de Moidrey reservoir; BA. Bec d'Andaine; D. Couesnon Dam; FC. Falaises (cliffs) de Champeaux; GB. Grand Banc; GS. Grouin du Sud; HB. Hermelles Bank; HC. Hermelles de

 doi:10.20944/preprints202305.1982.v1

Champeaux; HE. Herbus or schorre (East); HW. Herbus or schorre (West); M. Mont-Saint-Michel; MD. Mont Dol; PG. Pointe du Grouin; RT. Roche Torin; T. Tombelaine islet; I to IV. See text. a-b NW-SE profile (Figure 1).

2. Materials and Methods

2.1. Study site

The Mont-Saint-Michel Bay along the Channel is a megatidal embayment located in the north-western part of France [20–24]. It is spread over two French regions, Brittany to the west and Normandy to the east. The size of the bay is about 500 km², including 300 km² of tidal flats during the spring low tides and 40 km² of salt marshes locally called *les Herbus* (Figure 2). The Mont is in the south-eastern part of the bay, within an estuarine complex of about 80 km² mainly composed of the Couesnon, Sée and Sélune rivers (Figure 2). It is a circular granitic islet about 250 m in diameter, culminating at 46 m and capped by the Medieval abbey.

The bay has a semidiurnal tide, with a spring tidal range of about 13 m (exceptionally 14 m) and a neap tidal range of 4 m as observed at the Cancale gauge station. The water height varies during half a lunar month (about 29.5 days) separating two dead water slacks. Due to the barrier effect of the Cotentin peninsula, the ebb is always longer than the flood and this latter reaches high speed during spring tides (up to 4 m/s). Tidal flats dominate up to about 15 km offshore. We discuss elsewhere that the satellite pass close to 11:00 UTC allows observing only a maximum of 80% of the tidal flats in the Mont-Saint-Michel Bay, because spring tides generally occur at about 02:30 PM UTC [25].

2.2. The sediments in the Bay

The Mont-Saint-Michel tidal flats include four main environments [22]. In the internal part of the embayment, the Mont and the Tombelaine islet are located within the estuarine complex where the outlets of the Sée, Sélune and Couesnon River estuaries converge. A lot of creeks drain waters from the salt meadows. The sediments are fine to very fine sand and calcareous sandy shelly mud locally known as the 'tangue' (I, Figure 2, see also Figure 1). In the centre, a tidal delta fan is the continuation of the estuarine complex. It is mainly composed of fine sand cut by large tidal channels (II, Figure 2). In the northeast part, close to the Bec d'Andaine, a sandy barrier beach extends between Saint-Jean-le-Thomas and Genêts (III, Figure 2). In the southwest part, particularly between Saint-Benoît-des-Ondes and Cherrueix, the bottom of the bay is very gently sloping. The sediments range from mud and silty sand to shell bars. The Hermelles Bank, a reef built by annelid worms, lies in the lower part of the tidal flat (IV, Figure 2).

2.3. Restoring the maritime character of Mont-Saint-Michel

For two centuries (1769-1969) all interventions contributed to the silting up of the bay and to the development of the polder surfaces [19,26]. The Couesnon River was channelized in 1863 (Figure 3, 1952, Cchl and Cchr) and the diking of the polders to the West of the Mont launched in 1769 was achieved in 1933 (d and pw). A tidal power plant project between Cancale and the Chausey islands situated 20 km off the coast was abandoned in the 1950s. A dam (*Barrage de la Caserne*) was built over the Couesnon River in 1969 (Figure 3, 1986, CaD), mainly to drain the surrounding marshes. The dam represented the last facility contributing to the silting-up.

The reestablishment of the maritime character of the Mont-Saint-Michel is a long-term operation. The question of the insularity of the Mont was put back in the agenda in 1966 during the celebration of the abbey's first millenium. Studies were launched as early as 1972 by the *Laboratoire central d'hydraulique de France* (LCHF). Recommendations resulted in considerable and wide-ranging works including two new dams, the storage of one million cubic meters of water in the restored Couesnon channel, two seven hundred thousand cubic meters reservoirs close to the coast and the restoration of the Guintre and Ruisseau Landais river mouths. The Roche Torin dike in the south-eastern part of the bay was cut flush in 1983-1984 but the other recommendations were not followed up. The *Mission*

Preprints (www.preprints.org) | NOT PEER-REVIEWED | Posted: 29 May 2023 doi:10.20944/preprints202305.1982.v1

du Mont-Saint-Michel created in 1989 considered new solutions based on a scale model developed by SOGREAH [27,28]. The works had to be concentrated around the Mont and more respectful of the environment. The political decision by the French government was taken in March 1995. The development phase including the public enquiry was completed in 2003 and identified the project's main potential effects on the environment. Works began only in 2007 when the meadows extension was critical, and the Mont seemed to be caught in a pincer (Figure 3, 2003).

The main facility is a new dam with flood tide gates over the Couesnon River completed as early as May 2009 (Figure 3, 2007, CoD). This dam replaces the 1969 dam and is associated to the 'Anse de Moidrey' upstream reservoir (Figure 2, AM), completed in 2014, to restore the Couesnon's hydraulic capacity and move sediment away from the Mont. In 2010-2013, a landscaped car park, reception and service buildings, the pedestrian footbridge (760 m long, pf) and the new causeway (1,085 m long, ncw) were built. Hydraulic developments downstream of the dam took place between 2011 and 2015, with the construction of the West channel in 2012 (Figure 3, 2015, Cwc) and East channel in 2015 (Figure 3, 2016, Cec) separated by a spur (sp) composed of the bulkheads formerly protecting the Couesnon riverbanks. In 2015, the main phase of the works was achieved with the destruction of the old causeway (dcw), which was built in 1879 and since then blocked the tidal currents and played a major role in silting-up around the Mont.

2.4. Previous remote sensing studies

The Mont-Saint-Michel Bay was used as a reference area for several remote-sensing experiments. A Spot image acquired in 1986 was the background for the geological mapping [22]. The Optical Sensor onboard JERS appeared able to detect carbonate responses, especially suspended particles in the turbid plumes [18]. The evolution between 1986 and 1995 surveyed with Spot images showed the development of the salt meadows [29]. The potential of optical satellite imagery compared to radar and aerial photographs has been also evaluated [30]. Seminal lidar works were carried out for the study of the vegetation of the schorre [31]. More recently, lidar data have been acquired close to the Mont to control the efficiency of the new facilities [32] and to study facies models for tidal point bars lacking a three-dimensional perspective [33].

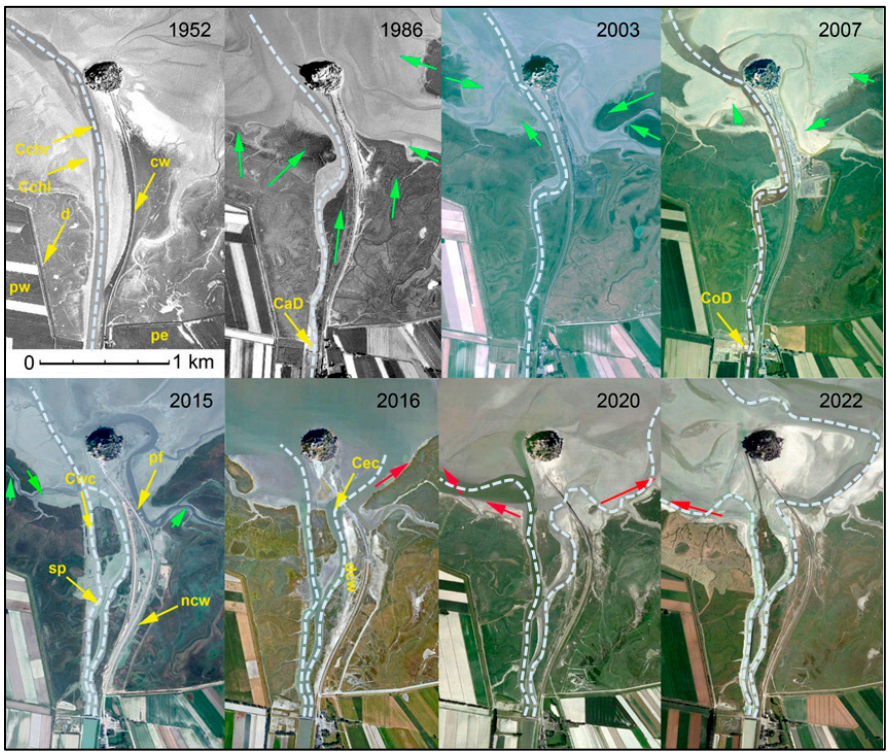

Figure 3. Evolution of the Mont from 1952 to 2022 (aerial photographs from Google Earth except for between 1952 and 1986): facilities and sedimentation. Red arrows: erosion of the schorre; green

 doi:10.20944/preprints202305.1982.v1

arrows: progradation of the schorre. Light-blue dashed lines: Couesnon watercourses. CaD: Caserne Dam (1969); Cchl: Couesnon channel left bank; Cchr: Couesnon channel right bank; Cec: Couesnon eastern channel (2015); CoD: Couesnon Dam (2007-2009); cw: causeway (1878-1879); Cwc: Couesnon western channel (2012); d: dike (1933); dcw: destroyed causeway (2015); ncw: new causeway (2012); pe: polder east (1946); pf: pedestrian footbridge (2013); pw: polder west (1934); sp: spur (2015).

2.5. The remote sensing approach

Aerial photographs are widely used (Figure 3) but the revisit time is too large (usually one to five years) for a regular survey. The method developed in the present approach deals with the use of time-series satellite images. Due to the size of the main features, only resolution (or pixel size) up to 20 m are considered. The survey of the environment of the Mont is carried out before, during, and after the facilities were built. These latter ranged from 2007 to 2015. Therefore, we used two data sets. The main data set is composed of 188 Sentinel 2 (109 S2A, 79 S2B) images from the European Space Agency satellites launched on 23 June 2015 (S2A) and 7 March 2017 (S2B), respectively. The selected S2 images were acquired between 1 August 2015, and 5 May 2023. These cloud free images present a 10 m resolution available for the blue, green, red and near IR ranges, or a 20 m resolution also including the red edge, mid- and short waves IR ranges. The images cover the whole post-work period (the eastern channel was achieved in May 2015) with a high revisit time, theoretically one image every 2.6 days in average, in the database, one image every 15 days in average because of the frequent cloud cover.

Four main products were used, the true colour composite (Red=red range i.e. S2-band 4; Green=green range i.e. S2-band 3; Blue=blue range i.e. S2-band 2), the standard false colour composite (Red=near infrared range i.e. S2-band 8; Green=red range i.e. S2-band 4; Blue=green range i.e. S2-band 3), a black-and-white image of the near infrared range (S2-band 8), and also a false colour composite at 20 m resolution including the infrared ranges (Red=near IR range i.e. S2-band 8A; Green=mid IR range i.e. S11-band 3; Blue=short waves IR range i.e. S2-band 12). The true colour composite is interesting for a global approach of the tidal flats, but it is sometimes difficult to accurately detect the vegetation front (especially in wintertime) and the water in the channels due to the turbidity. The standard false colour composite allows to detect the frontline of the schorre more easily, because the reflectance of vegetation is high in the near infrared, whatever the season of acquisition. The black-and-white image of the near infrared range is better for distinguishing between water and humid sediments. The IR false colour composite at 20 m resolution is useful for distinguishing between the waterbodies (black) and the land surfaces (clear), with the different kinds of vegetation in shades of red.

Aster images acquired onboard Terra, a joint mission within the NASA's Earth Science Enterprise launched on 18 December 1999, were used especially for the period prior to the works, although the sensor is still operating in 2023. Twelve images ranging from 7 April 2000 to 22 September 2017 were selected. The VNIR-sensor has 15 m resolution and required resampling and geometric correction to render the images in the same geometry as the S2 images. Due to the lack of the blue range, the true colour composite cannot be obtained with this sensor. The Aster standard false colour composite corresponds to Red=near infrared range i.e. Aster-band 3N; Green=red range i.e. Aster-band 2; Blue=green range i.e. Aster-band 1.

The ALOS-1 satellite was launched on 24 January 2006 and was **declared dead in orbit, 12 May 2011, after abruptly powering down that** turned off all the observation devices**.** ALOS carried three sensors: the Phased Array L-band Synthetic Aperture Radar (PALSAR), the Panchromatic Remote-Sensing Instrument for Stereo Mapping (PRISM), and the Advanced Visible and Near-Infrared Radiometer type 2 (AVNIR-2). This latter has been used in the present study. It comprised only four bands in the blue, green, red, and near IR ranges with a 10 m space-resolution. The scene acquired on 24 October 2007 was included in the database because it represents the lowest height of the sea at the time of acquisition (2.56 m) and fills the lack of Aster data at the time of the new dam construction. ALOS-2 launched in 2014 had optical cameras removed to reduce costs and ALOS-3 including an enhanced optical sensor was unsuccessfully launched in March 2023.

Preprints (www.preprints.org) | NOT PEER-REVIEWED | Posted: 29 May 2023 doi:10.20944/preprints202305.1982.v1

Other archive satellite data have been consulted, particularly Landsat Thematic Mapper (TM) images covering the four last decades with a resolution of 30 m.

All 201 satellite images have been brought together in a database comprising the date, the UTC hour, the sensor (Sentinel 2A, 2B, ALOS-AVNIR-2 or Terra-Aster), the flood, ebb or slack water status, the place in the half a lunar month cycle, the height of the sea provided by the French *Service Hydrographique et Océanographique de la Marine* (SHOM). A correction of the standard height is necessary by considering the actual atmospheric pressure at the time of acquisition [25]. A difference from the average *of* 1 hPa causes a difference *of* 1 cm in elevation (standard conditions are defined at 1,013.25 hPa). The actual pressure in the bay area ranges from 989 to 1,044 hPa, with an average value of 1,022 hPa (see also Supplementary materials).

Here, there is no quantitative approach of the reflectance values, but preliminary studies indicate different paths of research, for example the accurate analysis of the red edge range for vegetation mapping. The main objective of the project around the Mont is to avoid the islet to be joined to the surrounding salt meadows. Thus, a large part of the schorre to the west and to the east of the Mont should be eroded. The time-series is mainly used for manually or semi-automatically drawing the successive frontlines of the vegetation, and to survey the courses of the Couesnon channels, and those of the Sélune estuary as well. Finally, the main goal is to understand, whether the main hydraulic hypotheses are confirmed or not by the short-term evolution of the bay. From a methodological viewpoint, the database is used for identifying identical water elevation conditions but separated by a certain period. Due to very large meander divagation, it is difficult to use the classical waterline method [34] in the estuarine complex. Nevertheless, the method is evaluated here for detecting the movement of the banks and silting-up in the northeastern part of the bay.

The overall methodology is summarized in Figure 4.

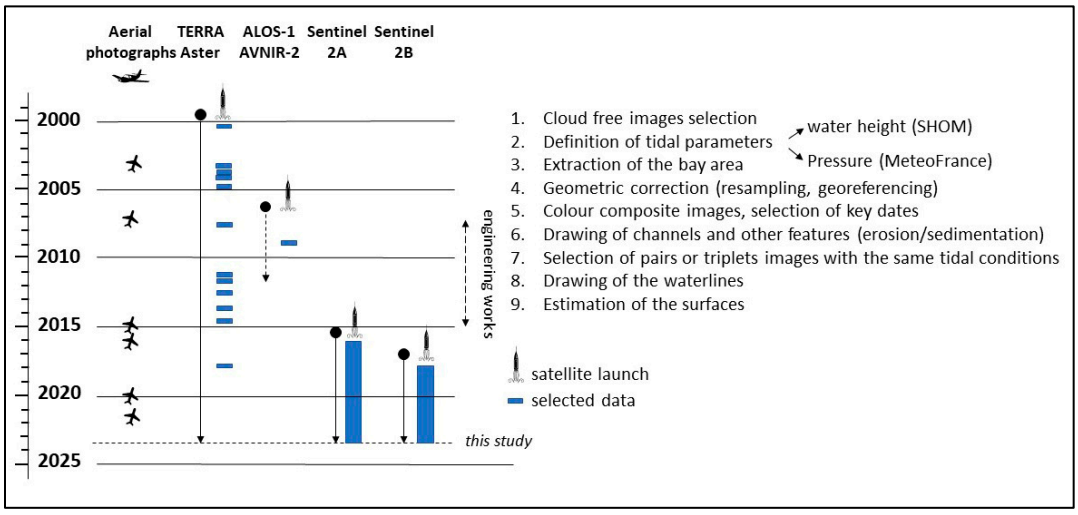

Figure 4. Methodology. Principle of image selection and main analytical steps.

3. Results

3.1. The schorre (vegetation frontline)

Thirteen satellite images have been selected to cover the period from 2000 to the present. Nine Sentinel-2 images cover the post-works period (2015-2023) with one image per year considering the first (1 August 2015) and one of the last (8 April 2023) available S2-images. Four other satellite images, Aster and ALOS, cover the 2000-2012 period, i.e., before and during the works. The schorre was surveyed according to four areas, the so-called polders W, MSM W, MSM E, and polders E (Figure 5). MSM W and MSM E are located at about 2 km from the Mont and are used to characterize the direct impact of the engineering works. Polders W and polders E allow surveying the global evolution at about 10 km to the west and 6 km to the east of the Mont.

Preprints (www.preprints.org) | NOT PEER-REVIEWED | Posted: 29 May 2023 doi:10.20944/preprints202305.1982.v1

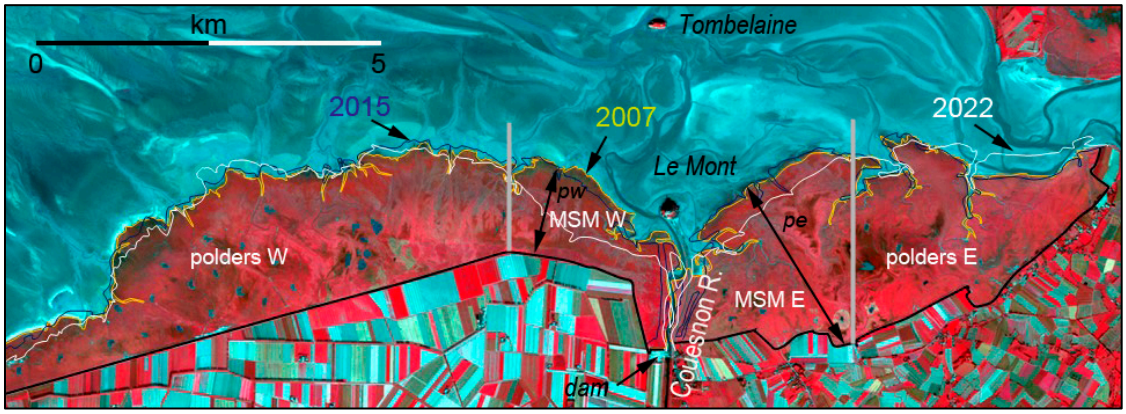

Figure 5. Survey of the schorre lines. Areas used for calculating the schorre surface (Table I). For readability, only three dates are illustrated (2007, 2015, 2022). The background image is the ALOS-AVNIR-2 false colour composite acquired on 24 October 2007. The Couesnon river constitutes the limit between MSM W and MSM E. The new facilities induce new schorre areas in the former course of the Couesnon (see 'Couesnon' in the Table). Pw and pe correspond to the profile for MSM-W and MSM-E, respectively.

In the period 2000-2007, the vegetation continued to expand and the schorre surface reached a maximum with about 2,621 ha (see 'Grand Total' in Table 1). All areas are characterized by accretion, except to local erosion phenomena along the polders W. Between the beginning of the works in 2007 and the present (2023), the erosion of the salt meadows has been significant to the south-west of the Mont (− 150 ha), but more limited to the south-east (− 65 ha). This erosion effect is restricted to the immediate environment. The vegetation fringe along the dike is slightly increasing to the west (+ 35 ha for polders W) and to the east (+ 40 ha for polders E). For the period 2000 to 2023, the increase is higher in both the polders west (+ 80 ha) and the polders east (+70 ha), illustrating the trend known since the construction of the last dikes in the 1930s.

Table 1. Surfaces of the 'schorre' surfaces expressed in ha. The dates are given according to yyyymmdd (see also Figure 4 for location).

Date	polders W	MSM-W	Total W	MSM-E	polders-E	Total E	Couesnon	Grand Total
20000407	1,077.2	254.4	**1,331.6**	488.1	571.5	**1,059.6**		**2,391.2**
20040909	1,199.6	281.1	**1,480.7**	511.5	551.7	**1,063.3**		**2,544.0**
20071024	1,194.8	285.7	**1,480.5**	535.9	604.5	**1,140.4**		**2,620.9**
20120526	1,176.0	259.8	**1,435.8**	501.3	606.8	**1,108.1**		**2,543.9**
20150801	1,214.0	251.3	**1,465.3**	493.7	628.7	**1,122.4**	14.5	**2,602.3**
20161031	1,225.0	243.4	**1,468.4**	518.6	616.7	**1,135.3**	9.7	**2,613.4**
20171113	1,213.8	225.0	**1,438.8**	502.9	621.2	**1,124.1**	12.6	**2,575.4**
20181021	1,224.7	214.3	**1,439.1**	508.5	629.9	**1,138.4**	8.7	**2,586.1**
20190919	1,226.6	190.6	**1,417.3**	489.5	641.3	**1,130.8**	9.2	**2,557.2**
20200913	1,236.7	178.2	**1,414.9**	466.7	661.2	**1,127.9**	9.3	**2,552.0**
20211008	1,236.6	162.6	**1,399.2**	475.6	664.6	**1,140.2**	10.2	**2,549.6**
20221020	1,217.9	150.2	**1,368.1**	448.3	684.1	**1,132.4**	9.0	**2,509.5**
20230408	1,228.9	132.5	**1,361.4**	469.2	644.3	**1,113.6**	7.5	**2,482.4**

Because the Couesnon River is divided in two channels since May 2015, some small islands developed in the central part ('Couesnon' in Table 1). These islands are covered by halophytic plant,

Preprints (www.preprints.org) | NOT PEER-REVIEWED | Posted: 29 May 2023 doi:10.20944/preprints202305.1982.v1

but they currently represent less than 10 ha and are deeply influenced by human activities (mowing, trampling, etc.).

3.2. Evolution of the channels

3.2.1. The western channel (Couesnon W, Figure 6)

The western channel corresponds to the former river course when the old causeway blocked any sedimentary transfer toward the east of the Mont. The western channel can occasionally erode the eastern area, as observed in May 2012 when the Couesnon river course circled the Mont and went along the eastern schorre for more than 500 m (image not presented here).

As early as 2016, the Couesnon W migrated toward the schorre and began a considerable erosion activity to the south-west of the Mont (see also 3.1). Since then, the watercourse is relatively stable, but a change has been observed in February 2023 with a new branch flowing straight to the north, running very close to the Tour Gabriel to the west of the Mont and joining the Sée-Sélune main estuary.

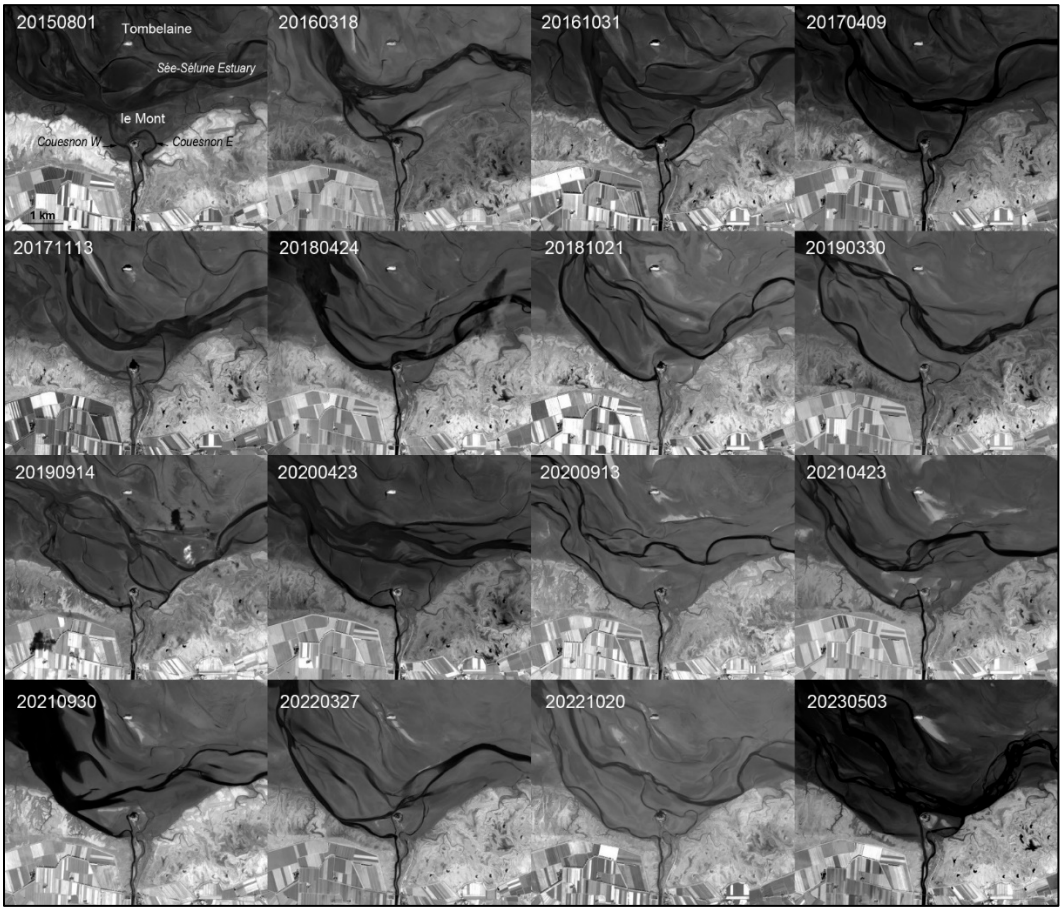

Figure 6. Time-series Sentinel-2 data from 2015 to 2023 illustrating the changes in the hydrographic network (Sée-Sélune and Couesnon rivers) close to the Mont-Saint-Michel. Black and white images of the near infrared range (band 8).

3.2.2. The eastern channel (Couesnon E, Figure 6)

Operating in May 2015, the eastern channel first went around the Mont and joined the course of the Couesnon W from the north and very close to the Mont. It contributed to the erosion of the eastern schorre from July 2016 onward. In early 2017, the channel migrated to the north-east, in the direction of the Sée-Sélune river, and the erosion of the schorre to the east of the Mont (MSM-E) ceased. Since then, the Couesnon E appears relatively limited. In late 2022, it shew a large meander flowing very

Preprints (www.preprints.org) | NOT PEER-REVIEWED | Posted: 29 May 2023 doi:10.20944/preprints202305.1982.v1

close to the Mont. The last image dated to early May 2023 indicates an unusual important watercourse, probably because of the rainy conditions prevailing for several weeks.

3.2.3. The Sée-Sélune estuary (Figure 6)

The Sée-Sélune estuary is not directly impacted by the new facilities but it plays a major role in the sedimentology of the estuarine complex. During the period from February to April 2018, the Sée-Sélune river migrated to the south and deeply eroded the schorre in the south-eastern part of the bay. This erosion concerned also the schorre to the east of the Mont. It ceased in late September 2018 when the Sée-Sélune river course headed north. The last images (from late 2022 onward) indicate a new migration of the Sée-Sélune to the south with the erosion of the Grand Banc (see also GB, Figure 2).

3.3. Sedimentary balance

The evaluation of the sedimentary balance necessitates to identify pairs or triplets of images acquired under the same hydrographic conditions, but on different dates and, if possible, the furthest apart in time. Only two pairs are presented here for illustrating the most important change (Figures 7 and 8).

Figure 7 shows the slikke (i.e. mineral) surfaces in 2015 and 2020, respectively, with the same corrected water heigh of 9.90 m and the same tidal conditions characterized by ebb tide about 5 hours and a quarter before the low tide, and the same place in the tidal cycle. In 2015, one of the first S2-image acquired on 21 August 2015 shows alternating tidal channels and banks between Tombelaine and the eastern coast. On 28 May 2020, five years after the last facilities were achieved close to the Mont, the area between Tombelaine and Grouin du Sud is totally covered by sediments. Tombelaine Island is now accreted to the coast. The main flood-tide channel between Bec d'Andaine and Tombelaine is still visible. The slikke surface to the north-east of the bay has increased from 672.5 ha to 1,402 ha.

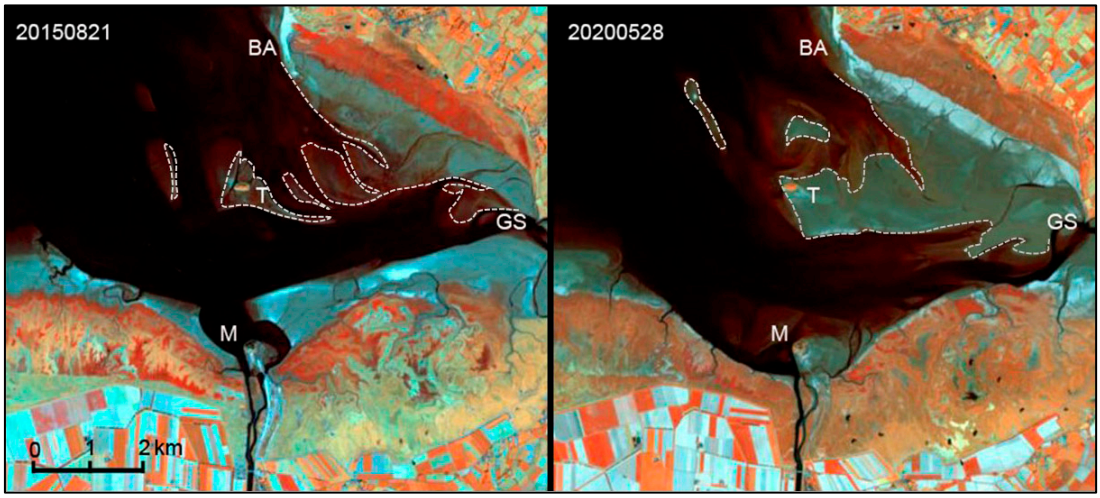

Figure 7. Comparison of two S2 colour composite using only the infrared ranges (Red=near IR i.e. band 8, Green=mid IR i.e. band 11, Blue=Short Waves IR i.e. band 12). The colour composite highlights the water bodies vs. land surfaces. BA: Bec d'Andaine, GS: Grouin du Sud, M: Mont-Saint-Michel, T: Tombelaine. The dashed lines correspond to the water height of 9.90 m.

Figure 8 shows the difference of the slikke surfaces in 2018 and 2023, with the corrected water heigh of 10.21 m and 10.23 m, respectively. The slikke surface to the north-east of the bay has increased from 705 ha to 1,328 ha. The change is probably slightly underestimated because of the 2 cm difference in elevation (10.23 m vs 10.21 m). The flood-dominated channel between Bec d'Andaine and Tombelaine is still visible but narrower. The silting-up of this area seems to accelerate within the last few years. Note that the trend is confirmed by the analysis of the intermediary image

Preprints (www.preprints.org) | NOT PEER-REVIEWED | Posted: 29 May 2023 doi:10.20944/preprints202305.1982.v1

acquired on 19 December 2020 with a water height of 10.21 m, not illustrated here for readability. The corresponding slikke surface is 930 ha. The erosion of the schorre close to the Mont seems to be acompanied by a large-scale silting-up in the internal part of the bay. If the erosion due to the Couesnon W along the schorre is evident, sediments are concentrating just west of the Mont (Figure 8, M, also confirmed in Figure 7).

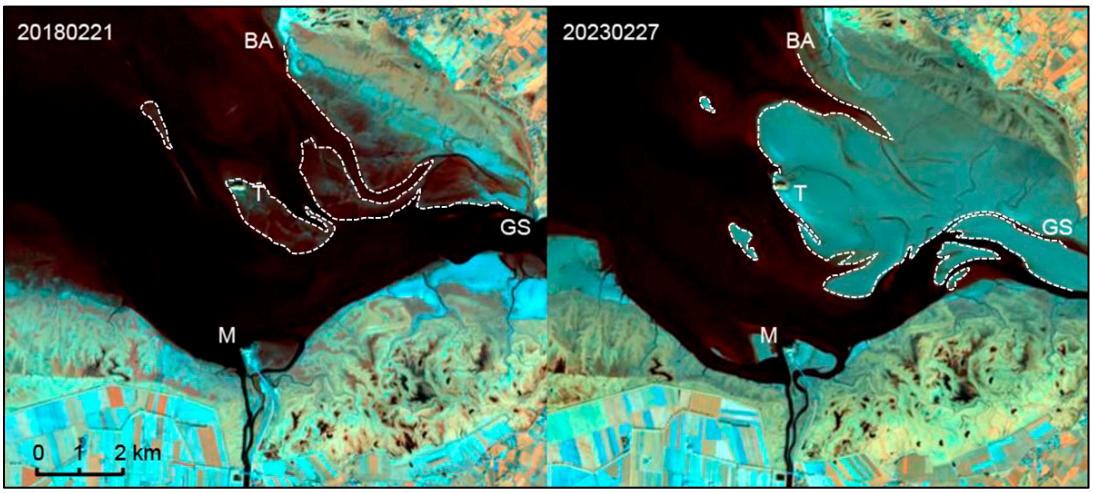

Figure 8. Comparison of two S2 colour composite (see Figure 7 for further explanations). The dashed lines correspond to the water height of 10.21-10.23 m. A large-scale silting-up of the northeastern part of the bay is observed between Bec d'Andaine (BA), Grouin du Sud (GS) and Tombelaine (T).

4. Discussion and conclusions

The main goal of the project of reestablishing the maritime character of the Mont-Saint-Michel is the islet to be surrounded by more high tides in the future. Eight years after the last facilities were built, the analysis of time-series satellite images indicates important erosion phenomena close to the Mont, particularly to the southwest due to the Couesnon West channel. Nevertheless, at about 3 km from the Mont, the vegetation surface (schorre) is stable or even tends to progress slightly, according to the trend that has prevailed for a century. Scouring and silting phenomena are clearly associated. Two main features must be discussed, the role of the vegetation and the new sedimentation conditions in the northeastern part of the bay, the evolution of which could be linked to the hydraulic works.

The type of vegetation plays a very important role along with the change in the hydraulic conditions. Basically, the engineering works act on different vegetal association. Considering the state of vegetation close to the Mont in 2007 [35], the salt meadows extent up to 2.6 km from the dikes to the east (Figure 6, pe) and about 1.4 km from the dikes to the west (Figure 6, pw). These distances are 2.3 and 0.4 km in 2023, respectively, illustrating the dramatic erosion of the western schorre. The slope is very small in both areas because the difference in height is only 3 m (maximum 12-13 m and minimum 9-10 m). The analysis of the satellite images and the field works show great changes in the vegetal associations. Three parts can be distinguished on a morphological basis (Figure 9).

The low marsh is dominated by the saltmarsh-grass (*Puccinellia maritima*) forming large grasslands. Some sea asters (*Tripolium pannonicum*) in the west and annual seablites (*Suaeda maritima*) in the east are mixed to the saltmarsh-grass. At the contact between the schorre and the sandy slikke, the glassworts (*Salicornia sp.*) and the common cordgrass (*Sporobulus anglicus* also known as *Spartina sp.*) act as pioneer plants. Particularly, the cordgrass sends out underground stems, which eventually form new clumps of grass. The dense root system binds mud, and the stems increase silt deposition. The density and the height of the cordgrass clumps are decreasing toward the sea. The common cordgrass is more frequent to the east of the Mont. Note that the pioneer area is frequently preceded by a hummocky zone.

Preprints (www.preprints.org) | NOT PEER-REVIEWED | Posted: 29 May 2023 doi:10.20944/preprints202305.1982.v1

The middle marsh is more regular and characterized by dense sea purslane (*Atriplex portulacoides*), a typical greyish-green shrub that grows to 75 cm. The species has also a high potential for sediment fixation. The sea aster to the east and the sea couch (*Elymus athericus*) to the west are also present.

The high marsh is more contrasted between the west and the east areas, probably due to the extensive sheep grazing to the east. In the latter area, the red fescue (*Festuca rubra*) is dominating. This plant presents narrow and needle like leaves, that makes it less palatable to livestock. The creeping bentgrass (*Agrostis stolonifera*), a perennial grass species forming extensive mats, is also present. To the west, there is a mixture of sea couch and red fescue. The sea purslane tufts are also frequent. The sea couch can tolerate harsh weather conditions. It is also a pioneer species generally associated with sand dunes not existing here because of the developments. The progression of the sea couch in this marsh area is spectacular as revealed by [36] indicating that it represented about 3% from the surface of salt marshes in 1984 and 45% in 2013. The main reason for this rapid evolution is the eutrophication due to the increase in nutrient levels in the waters of the bay coming from the watersheds including those of the Sée, Sélune and Couesnon rivers.

The results of the survey indicate that the low marsh has been totally eroded to the west between 2007 and 2023, along with about 75% of the middle marsh. On the contrary, only a small part of the low marsh has been eroded to the east of the Mont.

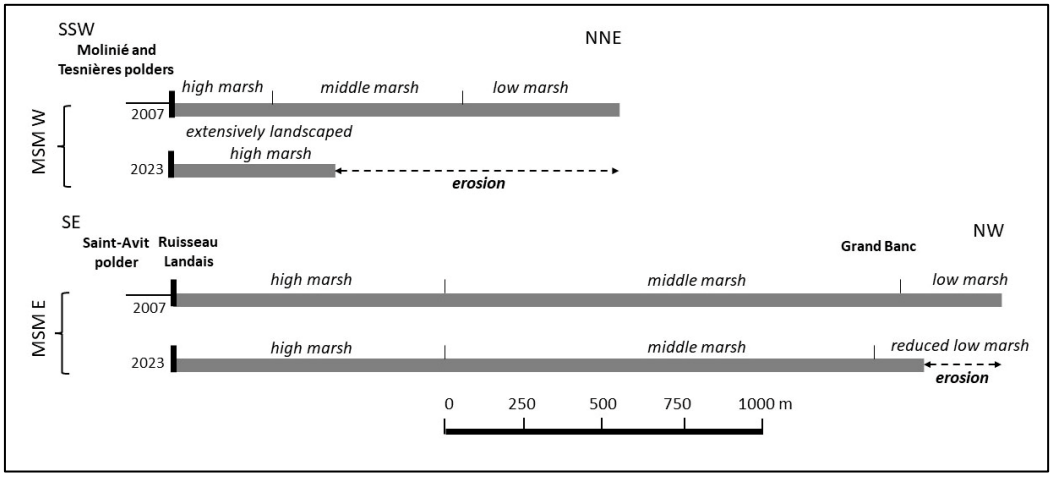

Figure 9. Sketch of the marsh in both the west and east zones on 2007 (beginning of the works) and 2023 (present-day setting) showing the differential erosion. The western area has been totally modified within the next few years by mowing and replanting works.

Because the comparison of Sentinel-2 images with the same tidal conditions is relevant for a short period (see for example chap. 3.3), ancient satellite data from the classical Landsat 5 Thematic Mapper (TM) have been also analyzed for comparing dates separated by decades. The previous analysis indicates that only acquisitions with water height of at least 8.50 m must be selected among hundreds of TM-images to allow the key sector of Bec d'Andaine-Tombelaine-Grouin du Sud to be observed. Figure 10 illustrates the comparison of the Sentinel-2A image acquired on 28 October 2021 and the Landsat 5-TM image acquired on 27 September 1990. Both images were acquired in neap tide conditions, with a water height of 9.11 m in 1990 and 9.10 m in 2021. The ebb tide acquisition was about six hours before the low tide, corresponding to the beginning of the ebb.

Although the colour composites are elaborated with the same spectral ranges, major changes are observed. The vegetation of the schorre along the southern coast is obviously different. In 1990, the vegetation association is more homogeneous. The red colour reveals the reflectance of the dominating sea purslane. As already mentioned, the middle and high marsh zones have been invaded from the 1990s onward by the sea couch, a plant that is dry in autumn. The yellow/green colour in the 2021 colour composite represents the sea couch dominancy, whereas the shades of red indicate the sea purslane, an evergreen plant. Note that we compared with the Sentinel-2B image acquired on

Preprints (www.preprints.org) | NOT PEER-REVIEWED | Posted: 29 May 2023 doi:10.20944/preprints202305.1982.v1

30 September 2021 (approximately the same date than the 1990 image) to check that the one-month difference (end-September vs end-October) does not significantly influence the mapping of the vegetation.

The comparison reveals that, initially, the sediments were accumulated off Bec d'Andaine. In 1990, the main flood channel was located along the coast between Bec d'Andaine and Grouin du Sud. The tidal channel overflew to form a tidal wedge, due to the high-speed flood tidal current. A considerable scouring took place during the last decades. In 2021, the dynamics of the flood is totally modified. The main flood channel migrated southward, approximately at the location of the Sée-Sélune-River which currently acts also as the main ebb channel.

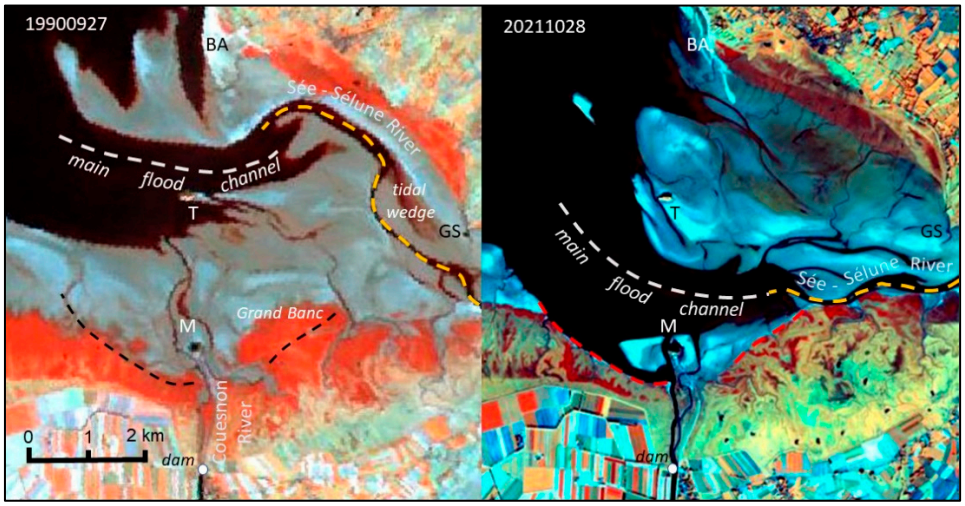

Figure 10. Mont-Saint-Michel. Comparison of two colour composite acquired in the same tidal conditions (neap tide, water height is 9.11 m in 1990 and 9.10 m in 2021, ebb tide about six hours before the low tide). The two dates are separated by 31 years. Only the infrared ranges are used. Left: Landsat-5 TM acquired on 27 September 1990 (Red=near IR i.e. band 4, Green=mid IR i.e. band 5, Blue=Short Waves IR i.e. band 7). Right: Sentinel 2A acquired on 28 October 2021 (Red=near IR i.e. band 8, Green=mid IR i.e. band 11, Blue=Short Waves IR i.e. band 12. BA: Bec d'Andaine, GS: Grouin du Sud, M: Mont-Saint-Michel, T: Tombelaine. Red dashed line: main erosion lines in 2021; black dashed lines: superimposition of the 2021 erosion lines. See text for details.

The influence of the human activities in coastal areas has been already investigated using remote sensing [37–41]. However, human rarely act so significantly on the hydrosedimentary balance in an embayment. Figure 11 illustrates the status of the major facilities in 2023 and a comparison with the initial setting in 2007, at the very beginning of the works for reestablishing the maritime character of the Mont-Saint-Michel. Note that the Sentinel-2 image in Figure 8B has been acquired six days after the photograph in Fig. 11A was taken.

This easy-to-implement method could usefully complement airborne lidar surveys [32] which require a heavier implementation. The lidar survey allows quantifying the sedimentary budget but concerns only a small part of the bay close to the Mont. Further studies will be necessary to understand whether the silting-up in the Bec d'Andaine-Tombelaine-Grouin du Sud area is directly linked to the engineering works or corresponds to a mixture of anthropic and natural evolution of the embayment.

Preprints (www.preprints.org) | NOT PEER-REVIEWED | Posted: 29 May 2023 doi:10.20944/preprints202305.1982.v1

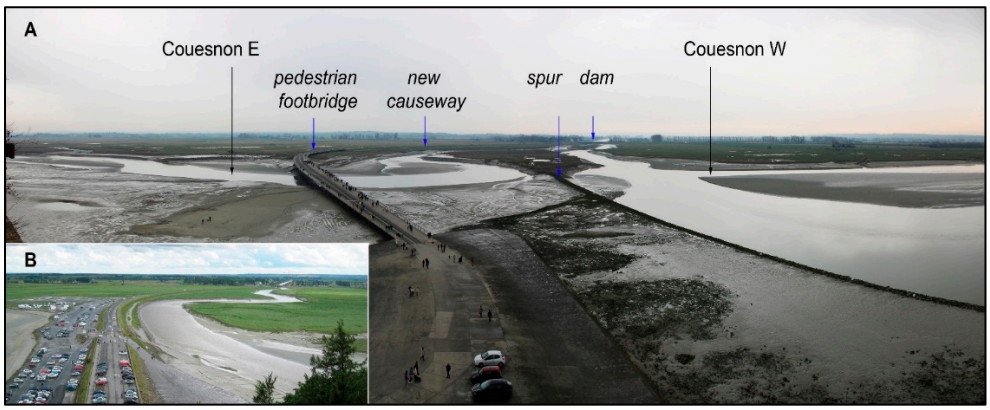

Figure 11. Photographs taken from the ramparts of the Mont-Saint-Michel (southward views). A. 21 February 2023. B. 31 May 2007. Cars were parked very close to the Mont in 2007. In the background, demolition work of the Caserne dam has begun (a construction crane is visible). The Couesnon river is largely meandering in the schorre and located only to the west of the causeway. The new facilities separate the Couesnon river in different parts (Couesnon east and west, channel along the spur) in 2023. The schorre has been partly eroded (see text for details).

4.4. Conclusions

In this paper, it was shown that chronicles of remote sensing images such as those acquired by the Sentinel-2 satellite system, already known in vegetation studies along the Couesnon River [42], are also very useful for monitoring erosion and accretion phenomena, particularly close to the Mont-Saint-Michel. Moreover, multi-temporal images acquired on the tidal flats of the Mont-Saint-Michel Bay could be successfully compared, when acquired under the same tidal conditions (water height, ebb or flood, same place in the tidal cycle, etc.). The correction of the standard height provided by tidal prediction is a very important point, particularly when in-situ measurements of the water level are not available. It is the case in the Mont-Saint-Michel, because the Cancale gauge station is located about 22 km to the west of the Mont. The human presence in the area and its relationship with the environment should be also studied as done elsewhere [43]. The remote sensing approach reveals important changes in the internal part of the bay, in the Bec d'Andaine-Tombelaine-Grouin du Sud area, even threatening the insularity of Tombelaine. These changes are likely related to the work for reestablishing the maritime character of the Mont. A regular survey involving field, aerial and satellite data is now necessary to verify that the secondary effects of the engineering project are not more severe than the expected results.

Supplementary Materials: The following supporting information can be downloaded at the website of this paper posted on Preprints.org.

Funding: This research was funded by the University Reims Champagne-Ardenne.

Data Availability Statement: The Sentinel 2 data have been downloaded from the Copernicus website (https://scihub.copernicus.eu) and Aster data from the dedicated website (https://gbank.gsj.jp). The ALOS-AVNIR-2 scene was obtained in the frame of a pilot-project of the Japanese Space Agency (JAXA).

Acknowledgments: The author would warmly thank all the students who contributed to the field investigations, particularly the Master students from the University of Bordeaux 3, and Yvette Marchand and Clélia Bilodeau, former PhD students. A special thanks to Irène Offermans for reviewing a preliminary English version. The author warmly dedicates this paper to his friend Professor Fernand Verger (1929-2018).

Conflicts of Interest: The author declares no conflict of interest. The funders had no role in the design of the study; in the collection, analyses, or interpretation of data; in the writing of the manuscript, or in the decision to publish the results.

References

1. Reed, D.J.; Davidson-Arnott, R.; Perillo, G.M.E. Estuaries, coastal marshes, tidal flats and coastal dunes. In *Geomorphology and Global Environmental Change,* Slaymaker, O., Spencer, T., Embleton-Hamann, C. (Eds.), Cambridge University Press, **2015**, pp. 130–152.
2. Semeniuk, V. Tidal flats. In *Encyclopedia of Coastal Science,* Finkl, C.W., Makowski, C., Eds; Springer Edit., **2019**, *36*, pp. 1708–1727.
3. Kang, Y.; Lei, J.; Wang, M.; Li, G.; Ding, X. Topographic evolution of tidal flats based on remote sensing: an example in Jiangsu coast, Southern Yellow Sea. *Front. Mar. Sci.* **2023**, 10:1163302.
4. Cohen, M.C.L.; de Souza, A.V.; Liu, K.-B.; Rodrigues, E.; Yao, Q.; Pessenda, L.C.R.; Rossetti, D.; Ryu, J.; Dietz, M. Effects of Beach Nourishment Project on Coastal Geomorphology and Mangrove Dynamics in Southern Louisiana, USA. *Remote Sens*. **2021**, 13, 2688.
5. Brunetta, R.; Duo, E.; Ciavola, P. Evaluating Short-Term Tidal Flat Evolution Through UAV Surveys: A Case Study in the Po Delta (Italy). *Remote Sens*. **2021**, 13, 2322.
6. Cracknell, A. Remote sensing techniques in estuaries and coastal zones – an update. *Int. J. Remote Sens*., **1979**, *20*, 485–496.
7. Benveniste, J.; Mandea, M.; Melet, A.; Ferrier, P. Earth observations for coastal hazards monitoring and international services: A European perspective. *Surv. in Geophys.* **2020**, *41*, 1185–1208.
8. Murray, N.J.; Phinn, S.R.; DeWitt, M.; Ferrari, R.; Johnston, R.; Lyon, M.B.; Clinton, N.; Thau, D.; Fuller, R.A. The global distribution and trajectory of tidal flats. *Nature* **2019**, *565*, 222–225.
9. Gawehn, M.; van Dongeren, A.; de Vries, S.; Swinkels, C.; Hoekstra, R.; Aarninkhof, S.; Friedman, J. The application of a radar-based depth inversion method to monitor near-shore nourishments on an open sandy coast and an ebb-tidal delta. *Coast. Eng*, **2020**, *159*, 103716.
10. Kohlus, J.; Stelzer, K.; Müller, G.; Smollich, S. Mapping seagrass (Zostera) by remote sensing in the Schleswig-Holstein Wadden Sea. *Estuar. Coast. Shelf Sci*., **2020**, *238*, 106699.
11. Madhuanand, L.; Philippart, C.J.M.; Wang, J.; Nijland, W.; de Jong, S.M.; Bijleveld, A.I.; Addink, E.A. Enhancing the predictive performance of remote sensing for ecological variables of tidal flats using encoded features from a deep learning model. *GIScience & Remote Sens*., **2023**, *60*, 1, 2163048.
12. Mason, D.C.; Scott, T.R.; Dance, S.L. Remote sensing of intertidal morphological change in Morecambe Bay, U.K., between 1991 and 2007. *Estuar. Coast. Shelf Sci*., **2010**, *87*(3), 487–496.
13. Ryu J.H.; Choi, J.K.; Lee, Y.K. Potential of remote sensing in management of tidal flats: A case study of thematic mapping in the Korean tidal flats. *Ocean & Coast. Management*, **2014**, *102*, 458–470.
14. Zhang, N.; Li, H.; Zhang, J.; Chen, J.; Wu, H.; Gong, Z. Study of the spatial and temporal distributions of tidal flat surface sediment based on multitemporal remote sensing. *Front. Mar. Sci*., **2023**, *10*, 1109146.
15. Tong, S. S.; Deroin, J. P.; Pham, T. L. An optimal waterline approach for studying tidal flat morphological changes using remote sensing data: A case of the northern coast of Vietnam. *Estuar. Coast. Shelf Sci.* **2020**, *236*, 106613.
16. Salameh, E.; Frappart, F.; Turkia, I.; Laignel, B. Intertidal topography mapping using the waterline method from Sentinel-1 & -2 images: The examples of Arcachon and Veys Bays in France. *ISPRS J. Photogramm. Remote Sens.* **2020**, *163*, 98–120.
17. Deroin, J.P.; Guillaneuf, A.; Laratte, S. A multisource approach for tidal flat study. Example of the Baie des Veys, Normandy, France. *Z. für Geomorph.* **2022**, *64* (1), 17–38.
18. Deroin, J.P.; Marchand, Y.; Auffret, J.P. Littoral survey using the JERS-OPS multispectral sensor. Example of the Mont Saint-Michel Bay (Normandy, France). *Remote Sens. Environ.* **1997**, *62*, 2, 119–131.
19. Verger, F. Marais de Dol et Baie du Mont-Saint-Michel. In *Zones humides du littoral français. Estuaires, deltas, marais et lagunes*, Belin Ed., Paris, 2009, pp. 177–201.
20. Phlipponneau, M. La Baie du Mont-Saint-Michel. Etude de morphologie littorale. Thesis, Faculty of Humanities, University of Paris, 1955.
21. Larsonneur, C. La Baie du Mont-Saint-Michel: un modèle de sédimentation en zone tempérée. *Bull. Inst. Géol. Bassin d'Aquitaine* **1989**, *46*, 5–73.
22. L'Homer, A.; Courbouleix, S.; Chantraine, J.; Deroin, J.P. Baie du Mont-Saint-Michel. *Geological map of France at 1:50,000,* BRGM, Ed., Orléans, **1999**, *208*, 184p.
23. Bonnot-Courtois, C., Caline, B., L'Homer, A., Le Vot, M. La Baie du Mont Saint-Michel et l'estuaire de la Rance. Environnements sédimentaires, aménagements et évolution récente. *Bull. Centres Rech. Explorat.-Product. Elf-Aquitaine*, Ed. Technip, Paris, **2002**, *26*, 256p.

24. Tessier, B.; Billeaud, I.; Lesueur, P. Stratigraphic organisation of a composite macrotidal wedge: The Holocene sedimentary infilling of the Mont-Saint-Michel Bay (NW France). *Bull. Soc. Geol. France* **2010**, *181*, 99–113.
25. Deroin, J.P.; Shimada, M. The importance of local mean time in remote sensing for mapping megatidal zones. *C. R. Geosci.* **2010**, *342*, 11–18.
26. Verger, F. Colmatage et génie civil aux environs du Mont-Saint-Michel. *Mappemonde* **2001**, 63, 25–28.
27. Viguier, J.; De Croutte, E.; Hamm, L. Hydrosedimentary studies to restore the maritime character of Mont-Saint-Michel. *Proc. Coast. Eng. Conf.* **2003,** 3285–3297.
28. Migniot, C.; Viguier, J. The silting-up around Mont-Saint-Michel and the method used to maintain its maritime character. In: Bonnot-Courtois, C., Caline, B., L'Homer, A., Le Vot, M. (Eds.), La Baie du Mont Saint-Michel et l'estuaire de la Rance. Environnements sédimentaires, aménagements et évolution récente, 2002, *Bull. Centres Rech. Explorat.-Product. Elf-Aquitaine*, Ed. Technip, Paris, pp. 125–152.
29. Marchand, Y.; Deroin, J.-P.; Auffret, J.-P. Morphodynamics of the Mont Saint-Michel Bay (West France) since 1986 by remote sensing data. *C. R. Acad. Sci. Paris* **1998**, *327*, 155–159.
30. Deroin, J.P.; Verger, F. Application of remote sensing to monitor the Mont-Saint-Michel Bay (France). *Spec. Pap. Europ. Space Agency* **2002**, *515*, 1–4.
31. Bilodeau, C.; Deffontaines, B.; Deroin, J.P.; Radureau, A.; Cohen, M. Estimation du potentiel des données LIDAR multi-échos pour l'étude de la végétation des marais salés : étude du biais des données LIDAR acquises au-dessus de la baie du Mont Saint-Michel et recherche d'une méthode de correction. *Revue Soc. Franç. Photogramm. Télédétect.* **2010**, *192*, 189–190.
32. Levoy, F.; Anthony, E.J.; Dronkers, J.; Monfort, O.; Montreuil, A.L Short-term to decadal-scale sand flat morphodynamics and sediment balance of a megatidal bay: Insight from multiple LiDAR datasets. *J. Coastal Res*. **2019**, 88, 61–76.
33. Cosma, M.; Lague, D.; D'Alpaos, A.; Leroux, J.; Feldmann, B.; Ghinassi, M. Sedimentology of a hypertidal point bar (Mont-Saint-Michel Bay, north-western France) revealed by combining lidar time-series and sedimentary core data. *Sedimentol.* **2022**, *68*, 1179–1208.
34. Mason, D.C.; Amin, M.; Davenport, I.J.; Flather, R.A.; Robinson, G.J.; Smith, J.A. Measurement of recent intertidal sediment transport in Morecambe Bay using the waterline method. *Estuar. Coast Shelf Sci*. **1999**, *49*, 427–456.
35. Détriché, S.; Susperregui, A.S.; Feunteun, E.; Lefeuvre, J.C.; Jigorel, A. Interannual (1999-2005) morphodynamic evolution of macro-tidal salt marshes in Mont-Saint-Michel Bay (France). *Cont. Shelf Res*. **2011**, *31*, 611–630.
36. Canard, A.; Prigent, L., Ysnel, F.; Robin, T.; Carpentier, A.; Lefeuvre, J.C.; Bioret, F. Le Mont-Saint-Michel et sa baie peuvent-ils se réconcilier? Documents phytosociologiques - Actes du colloque de Bailleul 2017 « Valeurs et usages des zones humides », **2019**, *12*, 114–122.
37. Tian, Q.; Wang, Q.; Liu, Y. Geomorphic change in Dingzi Bay, East China since the 1950s: impacts of human activity and fluvial input. *Frontiers of Earth Sci.* **2017**, *11(2)*, 385–396.
38. Blum, M.D.; Roberts, H.H. Drowning of the Mississippi Delta due to insufficient sediment supply and global sea-level rise. *Nature Geosci.* **2009**, *2(7)*, 488-491.
39. Kang, Y.; He, J.; Wang, B.; Lei, J.; Wang, Z.; Ding, X. Geomorphic Evolution of Radial Sand Ridges in the South Yellow Sea Observed from Satellites. *Remote Sens.* **2022**, *14* (2), 287.
40. Wang, Y.; Gao, S.; Jia, J.; Thompson, C.E.; Gao, J.; Yang, Y. Sediment transport over an accretional intertidal flat with influences of reclamation, Jiangsu coast, China. *Marine Geol.* **2012**, *291*, 147–161.
41. Xiucheng, Y.; Zhe, Z.; Shi, Q.; Kroeger, K.D.; Zhiliang, Z.; Covington, S. Detection and characterization of coastal tidal wetland change in the northeastern US using Landsat time series. *Remote Sens. Environ.* **2022**, *276*, 113047.

 doi:10.20944/preprints202305.1982.v1

42. Rapinel, S.; Mony, C.; Lecoq, L.; Clément, B.; Thomas, A.; Hubert-Moy, L. Evaluation of Sentinel-2 time-series for mapping floodplain grassland plant communities. *Remote Sens. Environ* **2019**, *223*, 115–129.
43. Nieuwhof, A.; Bakker, M.; Knol, E.; de Langen, G.J.; Nicolay, J.A.W.; Postma, D.; Schepers, M.; Varwijk, T.W.; Vos, P.C. Adapting to the sea: Human habitation in the coastal area of the northern Netherlands before medieval dike building. *Ocean and Coast. Management* **2019**, *173*, 77–89.